Not to appear in Nonlearned J., 45.

Evidence of the Exponential Decay Emission in the *Swift* Gamma-ray Bursts

T. Sakamoto[1,2], J. E. Hill[3,4], R. Yamazaki[5], H. A. Krimm[3,4], G. Sato[1,6], S. Swindell[7], K. Takami[5], J. P. Osborne[8]

ABSTRACT

We present a systematic study of the steep decay emission of gamma-ray bursts (GRBs) observed by the *Swift* X-Ray Telescope (XRT). In contrast to the analysis in recent literature, instead of extrapolating the data of Burst Alert Telescope (BAT) down into the XRT energy range, we extrapolated the XRT data up to the BAT energy range, 15–25 keV, to produce the BAT and XRT composite light curve. Based on our composite light curve fitting, we have confirmed the existence of an exponential decay component which smoothly connects the BAT prompt data to the XRT steep decay for several GRBs. We also find that the XRT steep decay for some of the bursts can be well fitted by a combination of a power-law with an exponential decay model. We discuss that this exponential component may be the emission from an external shock and a sign of the deceleration of the outflow during the prompt phase.

Subject headings: gamma rays: bursts

---

[1]NASA Goddard Space Flight Center, Greenbelt, MD 20771

[2]Oak Ridge Associated Universities, P.O. Box 117, Oak Ridge, Tennessee 37831-0117

[3]CRESST NASA Goddard Space Flight Center, Greenbelt, MD 20771

[4]Universities Space Research Association, 10211 Wincopin Circle, Suite 500, Columbia, MD 21044-3432

[5]Department of Physics, Hiroshima University, Higashi-Hiroshima, Hiroshima, 739-8526, Japan

[6]Institute of Space and Astronautical Science, JAXA, Kanagawa 229-8510, Japan

[7]Department of Physics, North Carolina Agricultural and Technical State University, 1601 East Market Street,Greensboro, North Carolina 27411

[8]Department of Physics and Astronomy, University of Leicester, LE1, 7RH, UK

1. Introduction

The transition between the Gamma-ray burst (GRB) prompt emission and the afterglow has generated great interest in the scientific community. It is believed that the GRB prompt emission is due to the internal shocks of accelerated particles, whereas, the afterglow is believed to originate from an external shock with a circum-burst medium (Rees & Mészáros 1994; Sari & Piran 1997; Mészáros & Rees 1997). During the GRB episode there should be a transition from one phase to the other, however, it is still an open issue as to when this transition occurs.

The Burst and Transient Source Experiment (BATSE) observation of GRB 980923 showed ∼400 s long lasting tail emission which is best described by a power-law temporal decay (Giblin et al. 1999). Based on the spectral and temporal characteristics of this burst, Giblin et al. (1999) concluded that the tail emission was part of the afterglow emission, thus, the external shock could be generated during the prompt γ-ray phase. Giblin et al. (2002) performed a systematic study of the prompt tail emission using 40 GRBs observed by BATSE. They found that the temporal decays are best described by a power-law with a decay index of -2 rather than an exponential. There are several other works with the BATSE data reaching to the same conclusion (e.g., Ryde & Svensson 2002).

According to the BeppoSAX observations, the late time afterglow smoothly connects with the prompt emission if the onset time of the light curve is defined as the start time of the last pulse observed in the Wide Field Camera (2–30 keV) (e.g., Pian et al. 2001; Piro et al. 2005). These observations support the idea that the late X-ray spike represents the onset of the afterglow. However, a few hours to a few days delay in pointing the narrow field X-ray instrument to the GRB position, weakens the discussion about the transition from the prompt emission to the afterglow.

Thanks to the revolutionary features of *Swift* (Gehrels et al. 2004), our understanding of the X-ray properties of GRBs has been improved dramatically. With the combination of the accurate on-board calculation of the GRB position by the Burst Alert Telescope (BAT:15-150 keV; Barthelmy et al. 2005) and the fast slewing capability of the spacecraft, *Swift* can start a highly sensitive X-ray observation with the X-Ray Telescope (XRT:0.2-10 keV; Burrows et al. 2005) within a few tens of seconds to a few hundred seconds of the burst trigger. According to the XRT observations, the X-ray properties of the GRB emission have very complex features (Nousek et al. 2006; Zhang et al. 2006). One of the striking discoveries by the XRT is the existence of the steep decay component during the initial phase of the X-ray light curve. The origin of this steep decay component is generally considered to be a result of the delayed prompt emission from different viewing latitudes of the jet, the so called "curvature effect" (e.g. Fenimore et al. 1996; Kumar & Panaitescu

2000). Tagliaferri et al. (2005) and Barthelmy et al. (2006) investigated the steep decay component with the composite BAT and XRT light curve for several GRBs. To generate the composite light curve, both papers performed an extrapolation of the BAT mask-weighted (background subtracted) light curve into the XRT 0.2–10 keV energy band using a best-fit power-law photon index. The authors found that GRB 050126 and GRB 050219A do not show continuous emission from the BAT to the XRT light curve (Tagliaferri et al. 2005), however, GRB 050315 and GRB 050319 do display a smooth continuation from the BAT to the XRT light curve (Barthelmy et al. 2006).

O'Brien et al. (2006) performed a systematic study of the early X-ray emission using a sample of 40 *Swift* GRBs. They constructed a composite BAT and XRT light curve in the 0.3–10 keV band. In order to extrapolate the BAT data points down to the 0.3–10 keV band, the BAT mask-weighted count rate was converted to flux in the 0.3–10 keV band using the mean of the BAT and the XRT best fit photon index obtained from a simple power-law model. A fit of the 40 GRB superimposed light curves in the 0.3-10 keV band can described by an exponential followed by a power-law decay.

To date, most of the BAT and XRT composite light curves have been produced from an extrapolation of the BAT data down into the XRT energy range using the BAT mask-weighted count rate with a best-fit photon index derived from a simple power-law model. However, we believe that this method could introduce systematic errors in the extrapolated flux for the following reasons. First, the BAT best-fit photon index may not represent the true photon index in the X-ray range. According to the BAT spectral simulation study, BAT is unlikely to measure the curvature ($E_{\rm peak}$) in the prompt emission spectrum for the majority of the bursts due to its relatively narrow energy range (Sakamoto et al. in preparation). Based on the observations from other GRB instruments, the photon index of the X-ray spectrum is well centroided around -1 (e.g. Sakamoto et al. 2005; Kaneko et al. 2006). In comparison, the distribution of the BAT time-averaged photon index from a simple power-law fit peaks around -1.5 (Angelini et al. in preparation). This clearly shows that the steeper photon index of the BAT spectra is due to the combination of a low-energy photon index of ~ -1 and a curvature in the spectrum. The top panel of figure 1 illustrates this problem. Because of the systematically steeper photon index of the BAT, if $E_{\rm peak}$ is within the BAT energy range, the extrapolated flux in the XRT energy range will be systematically higher (see also bottom panel of figure 1). Second, the spectral evolution during the prompt emission is not taken into account for most extrapolations of the BAT data. Most of the current analysis is using the same photon index derived from a simple power-law fit to the whole prompt emission (time-averaged spectrum) for all of the data. It is a well known fact that $E_{\rm peak}$ shifts from hundreds of keV to a few keV during the prompt emission (e.g. Frontera et al. 1999). This suggests that the photon index in the X-ray range

could change from -1, in the case when $E_{\rm peak}$ is well above the X-ray range, to -2.5 in the case when $E_{\rm peak}$ is well below the X-ray range. Without taking the spectral evolution during the prompt emission into account in the analysis, the error in the extrapolated flux in the X-ray range could be significant. Third, since the BAT mask-weighted count rate does not correct for the energy dependence of each photon, the count rate of the source in the off-axis direction will be systematically smaller than the on-axis case. According to the BAT Crab observation, the count rate from the Crab is $\sim$15% smaller in the 45 degree off-axis case. This off-axis effect is correctly taken into account in the BAT energy response matrix, but not for the BAT mask-weighted count rates. Therefore, unless one applies an additional off-axis correction to the BAT mask-weighted count rates, a systematically smaller flux is obtained if the source is in the off-axis direction, which is always true for the BAT GRB data prior to the spacecraft slewing to the GRB position.

We estimate the error which could be introduced in the extrapolation of the BAT data into the XRT energy range using the real data obtained from GRB 060124; the bottom panel of figure 1 shows the light curve of the prompt emission. Since the BAT triggered on the precursor, the spacecraft slew was complete before the main prompt emission started for this burst. Thus, this burst provides the opportunity to calculate the flux of the prompt emission without the need for any extrapolation into the XRT energy range. The extrapolation of the BAT data is performed in the same way as described in O'Brien et al. (2006). As seen in the figure, when the BAT mask-weighted count rate is extrapolated into the XRT energy range with a fixed photon index, the extrapolated flux can be over estimated by about a factor of four in this case compared to the actual flux, even in the on-axis case. Moreover, without taking the spectral evolution of the prompt emission into account, the shape of the light curve could also be incorrect.

Based on these systematic problems in the extrapolation of the BAT data down to the XRT energy range, we adopt a different approach to derive the composite BAT and XRT light curve. Instead of extrapolating the BAT data, we extrapolate the XRT data up to the BAT energy range. Our approach is to construct the composite GRB light curve of from the BAT and the XRT in the 15–25 keV energy range. There are several merits in this approach. According to calculations of the GRB synchrotron shock emission spectra (Sari et al. 1998), if the observed count spectrum has a photon index steeper than -2, and a power-law index of an electron distribution, p, steeper than 2 (where $\mathrm{N}(\gamma_e) \propto \gamma_e^{-p}$, and γ_e is the Lorentz factor of the electrons), then the observed frequency should be above the synchrotron critical frequency for electrons with a minimum Lorentz factor (ν_m) in the fast cooling phase or above the cooling frequency (ν_c) in the slow cooling phase. In this case, since there is no characteristic frequency above ν_m (in the fast cooling case) and ν_c (in the slow cooling case), it is reasonable to extrapolate upwards in energy. The electron power-

law index $p \geq 2$ is typical for both the prompt emission (e.g., Kaneko et al. 2006) and the afterglow of GRBs (e.g., Panaitescu & Kumar 2002; Yost et al. 2003). In addition, in the BAT analysis we performed a time-resolved spectral analysis and calculated the 15–25 keV flux for each time interval directly from the spectral fitting process. In this way, we are also taking into account the spectral evolution during the prompt emission in the flux calculation.

2. Analysis

We looked at the XRT light curves of all GRBs between June 2005 [1] to September 2006. We selected 54 GRBs with an early phase power-law decay index steeper than -2 (t_0 taken as the BAT trigger time). For each of these GRBs, we analyzed the XRT data. We found a significant difference in the XRT spectrum between the very early phase (spectrum in the Window Timing (WT) mode) and the late phase (spectrum in the Photon Counting (PC) mode) exists at energies below 2 keV for the most of GRBs. To minimize the effects of the spectral evolution, the absorption, and uncertainties in the low energy response of the XRT, we use only data with energy greater than 2 keV for the XRT. This reduced the number of bursts in the sample significantly due to much fewer counts having energy greater than 2 keV. We selected those bursts which satisfied the following criteria: 1) having more than four data points in the 2–10 keV light curve in the early phase, 2) no multiple XRT flares in the early XRT light curve[2], and 3) 90% confidence interval of the photon index derived from the joint spectral analysis of the PC and WT data including -2.

As mentioned in Zhang et al. (2006), the definition of the offset time (t_0) is critical when you plot the early phase light curve. Traditionally, t_0 is defined as the trigger time of the GRB instrument; when the count rate exceeds some background level (rate trigger). However, the definition of the BAT trigger time is different. The trigger time of BAT is the start time of the foreground time interval of the image from which the GRB is detected on-board. Thus, to be comparable to a rate trigger time, we define t_0 as the start time of the prompt emission (start time of t_{100} interval) for the whole sample.

---

[1]Following onboard software updates to correct for uncontrolled temperature and bright Earth effects and micrometeorite damage.

[2]We do not exclude the bursts having the detection of the flare by the BAT data.

2.1. BAT analysis

The BAT analysis was performed using HEAsoft version 6.1.1 and CALDB version 2006-05-30. The event-by-event data were used for the analysis. The non-linear energy correction for each event was applied by `bateconvert`. The mask-weighting factors were calculated by `batmaskwtevt` using the onboard position. The detector enable and disable map was created by `bathotpix` combining the enable and disable map generated by the flight software. We created the BAT light curve by `batbinevt` in the full energy range (15-350 keV[3]) in 4 ms binning except for GRB 051109A (64 ms), GRB 060427 (1 s) and GRB 060923C (64 ms). We used larger binning for these three GRBs because of a low signal-to-noise ratio of the emission. The duration and the time intervals based on the Bayesian Block algorithm (Scargle 1998) were calculated by `battblocks`. The spectrum of each time interval was extracted by `batbinevt`. The energy response file was created by `batdrmgen`. If the time interval was during the spacecraft slew, we updated the keywords in the spectral file related to the energy response process by `batupdatephakw` and then created the energy response file for the time interval by `batdrmgen`. We applied systematic error vectors to the spectrum using `batphasyserr` prior to doing the spectral analysis. The spectral analysis was performed using Xspec 11.3.2.

The energy flux in the 15–25 keV band was calculated for each time interval directly from the spectral fitting process. The spectra from each time interval were fitted with a simple power-law model. According to the BAT GRB catalog (Angelini et al. in preparation), the detection threshold of the BAT in the 15–25 keV band is $\sim 10^{-9}$ ergs cm^{-2} s^{-1}. Based on this result, the 15–25 keV flux was treated as an upper limit when the calculated 15–25 keV flux was less then 10^{-9} ergs cm^{-2} s^{-1}. The upper limit was estimated from using the event-by-event data from the Crab nebula on-axis observation collected on 2005 March 24 (observation ID: 00050100016). According to this observation, the BAT can detect the Crab nebula in the 15–25 keV band at 5 σ in a one second exposure. Assuming that the BAT sensitivity is scaled as the square-root of the exposure time (Markwardt et al. 2005) and a canonical Crab flux of 5.3×10^{-9} ergs cm^{-2} s^{-1} in the 15–25 keV band, we calculated the BAT 5 σ upper limit in the 15–25 keV band from the following equation,

$$F(15-25\mathrm{keV})_{5\sigma} = \frac{5.3\times10^{-9}}{f_{pcode}}\, t_{exp}^{-0.5}\ (\mathrm{ergs\,cm^{-2}\,s^{-1}}). \quad (1)$$

Here t_{exp} is the exposure time and f_{pcode} is the partial coding fraction. Since our estimation of the 5σ upper limit is based on the on-axis Crab observation, f_{pcode} will correct for a source

[3]The coded mask is transparent to photons above 150 keV. Thus, photons above 150 keV are treated as a background in the mask-weighted method. The effective upper boundary is $\sim$ 150 keV.

observed in the off-axis direction.

For the time-averaged spectral analysis, we use the time interval from the emission start time to the emission end time (t_{100} interval). When the spacecraft slew occurred during the time interval, we created the response matrices for each five second period taking into account the position of the GRB in detector coordinates. We then weighted these response matrices by the five second count rates and created the averaged response matrices. Since the spacecraft slews about one degree per one second in response to a GRB trigger, we choose five second intervals to calculate the energy response for every five degrees.

2.2. XRT analysis

The 13 bursts meeting the criteria outlined in section 2 were processed using the HEAsoft tools version 6.1.1 including the latest *Swift* software (version 2.5a). The level 2 cleaned event files were produced from the `xrtpipeline` task version 10.4 using the standard screening criteria. The most recent response matrices in CALDB (version 8) and the ancillary response produced from `xrtmkarf` were used . The standard grades (Burrows et al. 2005) were used in the analysis; grades 0-2 and 0-12 for WT and PC mode, respectively.

Only WT and nominally the first three orbits of PC mode data (Hill et al. 2004, 2005) from the first observation segment (000) were analyzed, as these data cover the initial steep decay and in the canonical cases (Nousek et al. 2006) the transition to the flatter decay.

The nominal source extraction region for WT was a 40- pixel square and for PC mode an annular region with a 3 pixel inner radius and 25 pixel outer radius was used to account for the pile-up (when more than one X-ray occurs in a single pixel or adjacent pixels) when the XRT switches from WT mode to PC mode. Uncorrected count rate light curves were produced using the nominal extraction regions to verify that the data were not piled up; greater than 100 c/s in WT mode (Romano et al. 2006) and greater than 1.0 c/s in PC mode (Moretti, private communication.). The extraction regions were changed to account for the piled-up cases in accordance with Romano et al. (2006) and Moretti, i.e. by increasing the inner radius of the annulus in the case of PC mode and eliminating an inner square centered on the source for WT mode.

The hardness ratio ((2.0-10.0)keV/(0.5-2.0) keV) was extracted from the data using `xselect` to ensure that there was no significant spectral evolution. An exposure map was created from `xrtexpomap` to correct for the dead columns and hot pixels. `xrtmkarf` was used to create two ancillary response files. The first included corrections for losses in the wings of the point spread function (psf) and the center of the annulus, for the exposure and

for vignetting. The second ancillary response was created with no correction for losses.

The spectrum file was binned with a minimum of 20 counts/bin in order for χ^2 statistics to be valid for the spectral fitting. Xspec version 11.3.2 was used to perform a joint spectral fit of the WT and PC data from 2–10 keV using a simple power law model and the first ancillary response file. The 15–25 keV normalization obtained from the *pegpwrlw* model was used to extrapolate the XRT count rate into flux in the BAT 15–25 keV energy range. The count rate to flux conversion obtained in this manner is corrected for the psf losses. The fitting process was repeated using the second ancillary response file with the photon index frozen to the best-fit value obtained previously. The ratio of the two flux factors (normalization) obtained from the two fits was used to correct the 2–10 keV count rate for psf losses.

A light curve of the extrapolated 15–25 keV flux was created using the best-fit conversion factor from Xspec. Only light curve bins with greater than 90% exposure were used to limit errors incurred by instrument mode switching. The light curve was binned to have greater than 20 counts/bin.

2.3. Fitting a composite BAT and XRT light curve

To investigate the connection between BAT and XRT data points in the composite light curves, we first fit the initial part of the XRT data, where there was no strong spectral evolution, and then both the BAT and XRT data jointly. The fits were performed with a power-law model with a offset time (PLO),

$$F_{15-25\mathrm{keV}} = K_{pow}\,(t - t_0^{pow})^{-\alpha}, \tag{2}$$

where t_0^{pow} is a offset time, α is a decay index, and K_{pow} is the normalization, and with an exponential model (EXP),

$$F_{15-25\mathrm{keV}} = K_{exp}\,\exp(-\frac{t}{w}), \tag{3}$$

where w is the decay constant and K_{exp} is the normalization. We fixed t_0^{pow} to zero for the fit of only the XRT data. Finally, we fit the BAT and XRT data simultaneously in a combination of a power-law model with an exponential decay component (PLEXP),

$$F_{15-25\mathrm{keV}} = K_{pow}\,(t - t_0^{pow})^{-\alpha} + K_{exp}\,\exp(-\frac{t}{w}). \tag{4}$$

The time interval of fitting for only the XRT data is selected from the first XRT data point to the data before having a deficit from the PLO model with a offset time set to be

zero. For the joint BAT and XRT fitting, the time interval is from the first BAT data point to the XRT data before showing a residual from the PLO model. Otherwise, we stated as a footnote in table 1. The time intervals used in the light curve fitting are shown in the fourth column of table 1. Basically, the best fit model is selected based on χ^2 of the fit. However, because a PLO model will not fit the data before t_0^{pow}, the judgment between PLO and PLEXP is based on the eye inspection whether the model fit both the BAT and XRT data simultaneously or not.

3. Results

The left panels of figure 2–2 show the composite BAT (black data points in open circles) and XRT (red data points in open triangles) light curve in the 15-25 keV band overlaid with the best-fit light curve model. The best-fit light curve models are PLO (eq. (2)) as a dashed line , EXP (eq. (3)) as a dash-dotted line, and PLEXP (eq. (4)) with a solid line from top to bottom. The best-fit parameters of the light curves are summarized in table 1. The best fit model is labeled as a blue. The right panels of figure 2–2 from top to bottom show the BAT light curve in the 15-150 keV band, the BAT photon index based on the time-resolved spectral analysis, the XRT 2–10 keV count rate, and the XRT count rate ratio (2.0–10.0) keV/(0.5–2.0) keV. The best-fit spectral parameters based on the joint XRT WT and PC mode data using above 2 keV are summarized in table 2.

In the initial steep decay phase of the XRT light curve, it is very difficult to distinguish between PLO and EXP from the XRT data alone. Both models fit equally well for all of the bursts. However, the difference and the importance of the individual components become clear when the BAT data are included in the fit. An EXP model fits nicely for GRB 050814, GRB 050915B, GRB 060427 and GRB 060428B. A PLO or a PLEXP model is not required for these GRBs. For GRB 060923C, a PLO is the model best represented by the composite light curve. A PLEXP is the best model for all other GRBs. The best-fit parameters which we used in the systematic study presented on this section are shown in bold fonts in table 2.

First, we investigated the possibility of the curvature effect for those GRBs having a PLO component in the BAT and XRT light curve fit. According to the curvature effect (Fenimore et al. 1996; Kumar & Panaitescu 2000), there should be a relation between the decay index, α, and the XRT photon index, Γ_{XRT}, described by, $\alpha = 1+\Gamma_{XRT}$, if the curvature effect is the cause of the XRT steep decay. Figure 3 shows the correlation between α and Γ_{XRT} in our sample. The dashed line is the expected relationship from the curvature effect ($\alpha = 1+\Gamma_{XRT}$). Although GRB 060923C might be consistent with the expectation from the curvature effect, the majority of our sample is not following the expected relation. The

inconsistency with the curvature effect could be due to neglecting the spectral evolution during the steep decay in our analysis of the XRT data. Looking at the time evolution of the count rate ratio of our sample, we found a hard to soft evolution from 0.6 to 0.5 and from 0.6 to 0.4 is seen for GRB 060202 and GRB 060211A. These changes correspond to an evolution of the photon index from 1.5 to 1.7 and from 1.5 to 1.9 respectively according to the calculation by Xspec *fakeit* command using the detector and the ancillary response files created for each source region. Thus, the effect of the spectral evolution could be consistent with the expectation of the curvature effect for GRB 060211A and GRB 060202. However, we do not see a strong spectral evolution for other GRBs except for GRB 060418. Note that for GRB 060418, there is a strong evolution in the hardness during the episode at t_0+150 s that may cause an error in the extrapolated flux.

We find that most of the sample requires an EXP component to fit the BAT and XRT data simultaneously. Moreover, there are a handful of GRBs for which only an EXP can smoothly connect the BAT to the XRT data. Thus, we can conclude that some of the early steep decay observed by XRT is a continuation of the exponential decay tail of the prompt emission. Interesting characteristics can be found for the bursts where a PLEXP model is as the most representative model for the composite light curve. The dominant component of the XRT data 180 s after t_0 for GRB 060202 is an EXP. There is almost equal contribution from a EXP and a PLO components in the very initial XRT data for GRB 050803 and GRB 060109. Whereas, a PLO is a dominant component for GRB 051109A, GRB 060111B GRB 060211A, GRB 060306 and 060418B. This result clearly demonstrates that the XRT steep decay could be composed of at least two different components. Without careful consideration of both the BAT and the XRT data, it is not possible to distinguish between these two different components. It is important to note that O'Brien et al. (2006) also reached to the similar conclusion that the BAT and XRT composite light curve is composing an exponential decay which relaxes to a power-law decay.

For the bursts having an EXP component, we investigate the correlation between the exponential decay index, w, and the prompt emission properties derived from the BAT data (table 3). The results are summarized in figure 4. No correlation is found for the properties of the prompt emission except between w and the BAT T_{90} which is obvious because of the connection to the duration of the bursts for both parameters.

Based on our study, there is a strong indication that the steep decay component observed by the XRT is part of the prompt emission (e.g., Nousek et al. 2006; O'Brien et al. 2006). Thus, we calculate the fluence which may be missed by the BAT due to its sensitivity limit. This fluence was calculated by accumulating the flux of the best-fit light curve model obtained by the joint BAT and XRT data from the end of the emission detected by the BAT to 1000

seconds after t_0. Figure 5 shows the ratio of the percentage of the fluence in the tail emission which the BAT missed because of its sensitivity and the fluence recorded by the BAT. For 7 out of the 13 GRB in the sample, the fluence for this tail component is less than 15% of the fluence recorded by BAT. However, more than 15% of the fluence could be radiated below the BAT sensitivity limit for GRB 050915B, GRB 051109A, GRB 060202, GRB 060211A, GRB 060427, and GRB 060428B. This result gives rise to the question whether the fluence as measured by the γ-ray instrument reflects the true fluence of the prompt emission or not.

4. Discussion

We have presented the BAT and XRT composite light curves extrapolating the XRT data up to the BAT energy range for GRBs which have a steep decay component in the initial XRT data. Based on the simultaneous fit of both the BAT and XRT light curves, we have confirmed the existence of an EXP component which smoothly connects the BAT prompt emission to the XRT steep decay for several GRBs. We have also found that the XRT steep decay for some of the bursts can be well fitted by a PLEXP model.

A PLO component is most likely originated in an internal shock (so called, the curvature radiation or high-latitude emission associated with the last bright spike, Kumar & Panaitescu 2000; Nousek et al. 2006; Zhang et al. 2006; Yamazaki et al. 2006). Our results support the idea because the most of the XRT steep decay component smoothly connects with the last bright episode detected by the BAT (e.g. GRB 050803). The instantaneous emission from a uniform jet produces the decay index of $\alpha = 1 + \Gamma$ (Kumar & Panaitescu 2000). This formula was examined using the power-law decay index derived by a PLO model and the photon index based on the joint WT and PC spectral analysis of our sample. We find that the decay index is not consistent with the formula for the majority of our sample. One of the possible reasons for this inconsistency could be the spectral evolution in the XRT data (Zhang, Liang, & Zhang 2006). However, as discussed in section 3, the spectral evolution may not be responsible for this inconsistency. Liang et al. (2006) investigated the curvature effect as an origin of the XRT steep decay using the data set of O'Brien et al. (2006). They made the assumption that the XRT steep decay component is due to the curvature effect and investigated whether the time zero is consistent with the beginning of the bright episode. They concluded that most of the time zero of their sample was consistent with this picture. Main concern in their approach is that for fixed power-law decay index expected from the formula $\alpha = 1 + \Gamma$ with a shift of the offset time which makes it possible to fit any kinds of a decay index to the early XRT data. If a bright episode in the BAT data, which could contribute to the steep decay component, is simultaneously fit with the XRT data, as in our

approach, both the offset time and the decay index will be constrained by the data. It may be difficult to test definitely the curvature effect or the formula $\alpha = 1 + \Gamma$ without fitting XRT and BAT data simultaneously. Also, our conclusion may suggest that the structure of the jet is much more complex than a uniform jet (e.g. Yamazaki et al. 2006).

One interpretation of an EXP component is the presence of the external shock emission during the prompt phase. Fenimore & Ramirez-Ruiz (1999) studied the case of the co-existence of the emission from the external shock (deceleration of the initial shell) during the activation of the internal shocks. They showed that the smooth long lasting soft emission which arose from an external shock could overlay the light curve of the prompt emission. Moreover, according to the recent optical observation by Rapid Telescopes for Optical Response during the prompt emission of GRB 050820A, they found a smoothly decaying emission which does not correlate with the prompt spikes (Vestrand et al. 2006). Furthermore, GRB 050814 in our sample could be interpreted as a single pulse produced by the external shock because of its very smooth shape in the light curve from the BAT to the XRT data. If this interpretation is true, we might be observing the sign of the deceleration of the outflow during the prompt phase in the XRT steep decay emission.

Following the argument of Fenimore et al. (1996) and Fenimore & Ramirez-Ruiz (1999), we estimate the bulk Lorentz factor of our sample, assuming an EXP component is purely due to an external shock emission. Let us assume that an external shock starts its emission at the radius R_0. The external shock will be decelerated because of sweeping up the inter-stellar matter (ISM). The total energy of the central engine, E_0, can be expressed as, $E_0 = (4\pi/3)R_0 n_{\rm ISM} m_p c^2 \gamma_0^2$ where $n_{\rm ISM}$ is a density of the ISM, m_p is the proton mass, c is a speed of light, and γ_0 is a bulk Lorentz factor at R_0. The duration of the emission (ΔT) is determined by the radial time scale (Piran 1999) which is the difference of the arrival time of the photons emitted between R_0 and aR_0 ($a > 1$) to the observer, $\Delta T = [(a^4 - 1)/4](R_0/2\gamma_0^2 c)$. Therefore, a bulk Lorentz factor can be expressed as, $\gamma_0 = (32\pi m_p c^2/3)^{-1/8}[(a^4-1)/4]^{3/8}(E_0/n_{ISM})^{1/8}(c\Delta T)^{-3/8}$. There is a relationship between ΔT and the full width at half maximum (FWHM) of the pulse ($T_{1/2}$) in the form of, 0.22 ΔT = $T_{1/2}$, which is valid for a pulse shape of a fast rise, exponential decay (FRED) (Fenimore et al. 1996). Thus, once we know the redshift, since $T_{1/2}$ can be estimated from the best-fit parameters of an EXP component, we can calculate a bulk Lorentz factor as a function of $E_0/n_{\rm ISM}$. In the following arguments, we use a typical value of 2 for the parameter "a" (in this $a = 2$ case, ΔT is the radial time scale from R_0 to $2R_0$).

For bursts with unknown redshifts (except for GRB 050814, GRB 051109A and GRB

060418), we used the mean redshift of 2.4 for the Swift long GRBs [4]. We can derive a reasonable range of γ_0 from 143 to 350 and R_0 of $\sim 10^{16}$ cm assuming $E_0/n_{\rm ISM} = 1 \times 10^{52}$ erg cm^3 for the 12 GRBs in our sample (table 3). Although it is difficult to perform in our sample because of not having the measurements of both $E_{\rm peak}$ and redshift, it would be interesting to see the correlation between γ_0 and $E_{\rm peak}$ at the GRB restframe ($E^{\rm src}_{\rm peak}$). One of the advantage of using the Swift sample for this study is that soft GRBs, so called an X-ray Flash (XRF), are including in the sample because of the relatively softer energy response of BAT comparing to that of BATSE. In the dirty fireball model (Dermer et al. 1999), $E^{\rm src}_{\rm peak}$ has a strong dependency on the bulk Lorentz factor ($E^{\rm src}_{\rm peak} \propto \gamma_0^4$). The unified jet models from XRFs to GRBs such as the structured-jet model (Rossi et al. 2002), and the variable jet opening angle model (Lamb et al. 2006; Donaghy 2006) expect a positive correlation between $E^{\rm src}_{\rm peak}$ and a bulk Lorentz factor. In the off-axis jet model (Yamazaki et al. 2004), we would not expect any correlation between γ_0 and $E^{\rm src}_{\rm peak}$ because the Doppler factor will change as a function of a viewing angle but not γ_0. Another interesting theoretical model to discuss as the origin of XRFs is the case of a very high Lorentz factor (Mochkovitch et al. 2003; Barraud et al. 2005). According to this model, XRFs can be produced in a condition with a very high γ_0 (so called "clean fireball"), while classical GRBs has a moderate γ_0. Therefore, we would expect a negative correlation between $E^{\rm src}_{\rm peak}$ and the bulk Lorentz factor in this model. Some additional works, for example, to estimate $E_{\rm peak}$ from the Swift BAT data (Sakamoto et al. in preparation) and to estimate a redshift from the Swift data (e.g., Grupe et al. 2006) are encouraged to discuss the origin of XRFs in the Swift sample for the investigation of the correlation between γ_0 and $E^{\rm src}_{\rm peak}$.

Now, we argue that a PLO component is originated from an internal shock. In the case, we can estimate the lower limit of a bulk Lorentz factor with a following argument. We assume that the photons originated from an internal shock via the curvature effect and from an external shock arrive at the observer simultaneously. The observed time of the photon from an internal shock, T_{int}, can be expressed as, $T_{int} \sim (R_{int}/2c\gamma_{int})[1+(\gamma_{int}\theta)^2]$, where R_{int} is the radius where an internal shock emits, γ_{int} is a bulk Lorentz factor at R_{int}, and θ is the jet opening half-angle. On the other hand, the observed time of an external shock emission, T_{ext}, is expressed as, $T_{ext} \sim R_{ext}/(4c\gamma^2_{ext})$, where R_{ext} is the radius where an external shock emits and γ_{ext} is a bulk Lorentz factor at R_{ext} (Sari 1998). Applying the condition of $T_{int} \sim T_{ext}$ and also assume $\gamma_{int} \sim \gamma_{ext} \sim \gamma_0$, we have, $2R_{int}[1+(\gamma_0\theta)^2] \sim R_{ext}$. Whereas, $E^{\rm src}_{\rm peak}$ can be written as a function of θ and γ_0, $E^{\rm src}_{\rm peak}(\theta) \sim (2\gamma_0 h\nu'_0)[1+(\gamma_0\theta)^2] \sim [E^{\rm src}_{\rm peak}(\theta=0)]/(1+(\gamma_0\theta)^2)$, where $E^{\rm src}_{\rm peak}(\theta=0)$ is $E_{\rm peak}$ observed by the on-axis observer. In this case, $E^{\rm src}_{\rm peak}(\theta=0)$ corresponds to the observed $E_{\rm peak}$ multiplied by (1+z). Therefore, we can derive the relationship between

[4]http://heasarc.gsfc.nasa.gov/docs/swift/archive/grb_table/

R_{int}, R_{ext} and $E_{\rm peak}$ with following formula, $R_{ext}/2R_{int} \sim [E_{\rm peak}(\theta = 0)]/E_{\rm peak}(\theta)$. Since the observed photon index of the XRT steep decay emission of our sample is ~ 2 which suggests the observation of the spectrum above $E_{\rm peak}$ energy, it is reasonable to assume that the upper limit of $E_{\rm peak}(\theta)$ is in a few keV range. Hence, the condition will be, $R_{ext}/2R_{int} > [E_{\rm peak}(\theta = 0)]/E_{\rm peak}(\theta')$ where $E_{\rm peak}(\theta')$ is the upper limit of a few keV. If we use the angular spreading time (ΔT_{ang}) (Piran 1999) as the time scale of an internal shock, then, $R_{int} \sim 2c\gamma_0\Delta T_{ang}$. The radius of an external shock can be expressed as (same formula used in the previous discussion), $R_{ext} = (4\pi m_p c^2/3)^{-1/3}(E_0/n_{ISM})^{1/3}\gamma_0^{-2/3}$. Thus, γ_0 can be written as, $\gamma_0 > (1/4)^{3/8}(4\pi m_p c^2/3)^{-1/8}(E_0/n_{ISM})^{1/8}(c\Delta T_{ang})^{-3/8}[E_{\rm peak}(\theta = 0)/E_{\rm peak}(\theta')]^{-3/8}$. Because of the difficulty to measure $E_{\rm peak}$ from the BAT data, we only estimate a bulk Lorentz factor for GRB 050803 with the best assumption about $E_{\rm peak}$. In the case of GRB 050803, the duration of the last spike (the pulse at t_0+90 s) is $\sim$ 3 s. This duration can be set as ΔT_{ang} with taking into account the time dilation effect. Although it is not possible to extract the information about $E_{\rm peak}$ of this pulse from the BAT data, it is reasonable to assume $E_{\rm peak} \sim 100$ keV since the photon index in a simple power-law fit of the BAT data is -1.2 ± 0.2 which is close to the low energy photon index of the typical GRB spectrum ($E_{\rm peak}$ should be around or above the BAT upper energy range of 150 keV). Therefore, we use $E_{\rm peak}(\theta = 0)/E_{\rm peak}(\theta') \sim 100$. The lower limit of γ_0 of GRB 050803 is estimated to be 78 assuming the redshift of 2.4 (the mean redshift of the Swift long GRBs). As shown in this example, again, the measurements or estimations of both $E_{\rm peak}$ and redshift are crucial for calculating the lower limit of a bulk Lorentz factor in our picture.

Yamazaki et al. (2006) investigated the GRB prompt emission 100– 1000 seconds after the GRB trigger in the frame work of a multiple sub-shell model. According to their study, despite an angular inhomogeneity of the jet, the tail emission has a monotonic decay which resembles the XRT steep decay. In this context, if the jet has a core in which emission energy is confined densely compared with the outer region, the PLO decay component arising from an on-beam sub-shell may be overlaid by the off-beam core emission which causes the EXP decaying component. Takami et al. (2006) further extended their study, and in order to investigate the unknown jet structure, they proposed unique definitions of the decay index derived by unique definitions of the time zero and of the fitting interval of the observed light curve. They found that the decay index in their definitions should have a wide scatter in the case of the jet having a power-law like structure. Here, we calculated the decay index using our BAT and XRT composite light curve based on their definitions. Because of the difficulty of using exactly the same definition by time zero as proposed in Takami et al. (2006) (T_* in their paper), we defined the end of the BAT emission as T_*. We can fit our light curves using the proposed fitting interval for five GRBs in our sample (α_{tail} as a decay index, χ^2 and d.o.f. of the fits are shown in the last two columns of table 3). Our results based on a very small

sample show that the decay index is ranging from 0.6 to 3.0. However, both the size of the sample and the number of data points included in the light curve fit are very small because of using the XRT data only above 2 keV. There is another problem for reducing a number of sample such as an appearance of a shallow decay in the XRT data in the fitting interval. Unfortunately, it is hard to conclude the structure of a jet with our limited sample. Once we can increase the GRB sample, which is suitable for fitting a light curve with their unique definitions, we may be able to draw a conclusion about the jet structure of GRBs using the XRT steep decay component.

We presented a systematic study of the steep decay emission observed by the XRT. We constructed the composite light curves in the 15–25 keV band extrapolating the XRT data up to the BAT energy range. Based on the simultaneous fitting of the BAT and XRT data, we confirmed the existence of an EXP component for the most of the burst. We found that our sample is inconsistent with the relationship of the curvature effect, $\alpha = \Gamma + 1$, which is only valid in the case of the uniform jet. We argue that the EXP component could be the emission from the external shock which may indicate the deceleration of the initial shell during the prompt phase. We also discuss about the case of the prompt tail emission from the structured jet as an origin of the XRT steep decay.

We would like to thank A. P. Beardmore, G. Chincarini, C. Guidorzi, P. T. O'Brien and K. L. Page for valuable comments. This research was performed while T. S. held a NASA Postdoctoral Program administered by Oak Ridge Associated Universities at NASA Goddard Space Flight Center. R. Y. was supported in part by Grants-in-Aid for Scientific Research of the Japanese Ministry of Education, Culture, Sports, Science, and Technology 18740153.

REFERENCES

Barraud, C. et al. 2005, A&A, 440, 809

Barthelmy, S.D. et al. 2005, Space Sci. Rev., 120, 143

Barthelmy, S.D. et al. 2006, ApJ, 635, L133

Burrows, S.D. et al. 2005, Space Sci. Rev., 120, 165

Dermer, C.D., Chiang, J., & Mättcher, M. 1999, ApJ, 656

Donaghy, T. Q. 2006, ApJ, 645, 436

Dupree, A.K. et al. 2006, GCN Circ. 4969, http://gcn.gsfc.nasa.gov/gcn3/4969.gcn3

Fenimore, E.E., Madras, C.D., & S. Nayakshin 1996, ApJ, 473, 998

Fenimore, E.E. & Ramirez-Ruiz, E. 1999, Submitted to ApJ (astro-ph/9909299)

Frontera, F. et al. 1999, ApJS, 127, 59

Gehrels, N. et al. 2004, ApJ, 611, 1005

Giblin, T.W. et al. 1999, ApJ, 524, L47

Giblin, T.W. et al. 2002, ApJ, 570, 537

Grupe, D. et al. 2006, Submitted to ApJ (astro-ph/0612104)

Hill, J.E., et al. 2004, Proc. SPIE, 5165, 217

Hill, J.E., et al. 2005, Proc. SPIE, 5898, 313

Jakobsson, P. et al. 2006, in AIP Conf. Proc. 836, Gamma-ray bursts in the Swift era, ed. S.S.Holt, N. Gehrels, and J.A.Nousek (New York: AIP), 552

Kaneko, Y. et al. 2006, ApJS, 166, 298

Kumar, P. & Panaitescu, A. 2000, ApJ, 541, L51

Lamb, D.Q., Donaghy, T.Q., & Graziani, C. 2006, ApJ, 520, 335

Liang, E.W. et al. 2006, ApJ, 646, 351

Markwardt, C.B. et al. 2005, ApJ, 633, L77

Mészáros, P., & Rees, M. 1997, ApJ, 476, 232

Mochkovitch, R., Daigne, F., Barraud, C., & Atteia, J. L. 2003, in APS Conf. Ser. 312, Third Rome Workshop on Gamma-Ray Bursts in the Afterglow Era, ed. M. Feroci et al. (San Francisco: ASP), 381

Nousek, J.A. et al. 2006, ApJ, 642, 389

O'Brien et al. 2006, ApJ, 647, 1213

Panaitescu, A., & Kumar, P. 2002, ApJ, 571, 779

Pian, E. et al. 2001, A&A, 372, 456

Piran, T. 1999, Physics Reports, 314, 575

Piro, L. et al. 2005, ApJ, 623, 314

Quimby, R. et al. 2005, GCN Circ. 4221, http://gcn.gsfc.nasa.gov/gcn3/4221.gcn3

Rees, M., & Mészáros, P. 1994, ApJ, 430, L93

Romano, P., et al. 2006, A&A, 456, 917

Rossi, E., Lazzati, D., & Rees, M.J. 2002, MNRAS, 332, 945

Ryde, F. & Svensson, R. 2002, ApJ, 566, 210

Sakamoto et al. 2005, ApJ, 629, 311

Sari, R., & Piran, T. 1997, ApJ, 485, 270

Sari, R. 1998, ApJ, 494, L49

Sari, R., Piran, T., & Narayan, R. 1998, ApJ, 497, L17

Scargle, J. D. 1998, ApJ, 504, 405

Tagliaferri, G. et al. 2005, Nature, 436, 985

Takami, K., Yamazaki, R., Sakamoto, T. & Sato, G, submitted to ApJ

Vestrand, W.T. et al. 2006, Nature, 442, 172

Yamazaki, R., Ioka, K., & Nakamura, T. 2004, ApJ, 607, L103

Yamazaki, R., Toma, K., Ioka, K., & Nakamura, T. 2006, MNRAS, 369, 311

Yost, S. A., Harrison, F. A., Sari, R., & Frail, D. A. 2003, ApJ, 597, 459

Zhang, B. et al. 2006, ApJ, 642, 354

Zhang, B.B., Liang, E., Zhang, B. 2006 (astro-ph/0612246)

Table 1. Parameters of the light curve fits. Errors in the 68% confidence.

GRB	t_0 UT	Data‡	Fitting [s]	Power-law				Exponential		
				t_0^{pow}	α	$K_{\rm pow}$	χ^2/dof	w	$K_{\rm exp}$	χ^2/dof
050803	2005-08-03	XRT	100–147	$0^{\dagger}$	5.3 ± 0.7	17.4	6.6 / 5	22 ± 3	$3.8^{+4.0}_{-1.9} \times 10^{-8}$	7.3 / 5
	19:14:59.3	PL/EX	0–406	$87.2^{+0.3}_{-0.4}$	1.18 ± 0.07	$(1.1 \pm 0.3) \times 10^{-8}$	14.4 / 10	32.3 ± 0.9	$(8.4 \pm 0.7) \times 10^{-9}$	122.2 / 13
		PLE	0–406	$\mathbf{88.3^{+0.03}_{-0.05}}$	$\mathbf{0.87 \pm 0.03}$	$\mathbf{2.0 \times 10^{-9\dagger}}$	–	$\mathbf{26 \pm 1}$	$\mathbf{1.0 \times 10^{-8\dagger}}$	**22.0 / 12**
050814	2005-08-14	XRT	167–466	$0^{\dagger}$	3.6 ± 0.3	$4.1^{+6.2}_{-2.4} \times 10^{-2}$	11.7 / 20	71 ± 4	4.0×10^{-9}	23.7 / 20
	11:38:55.4	PL/EX	0–466	70.3	2.5	5.3×10^{-5}	10.3 / 21	$\mathbf{66 \pm 2}$	$\mathbf{(5.0 \pm 0.5) \times 10^{-9}}$	**27.7 / 23**
		PLE	0–466	44.5	1.6	$5.1 \times 10^{-8\dagger}$	–	62 ± 1	$5.8 \times 10^{-9\dagger}$	24.2 / 22
050915B	2005-09-15	XRT	158–228	$0^{\dagger}$	5.3 ± 0.8	1.3×10^{2}	10.7 / 5	36^{+6}_{-5}	$2.1^{+2.7}_{-1.2} \times 10^{-8}$	11.7 / 5
	21:22:56.6	PL/EX	7–228	21.3	2.1	4.0×10^{-6}	27.0 / 7	$\mathbf{33.2 \pm 0.6}$	$\mathbf{(3.0 \pm 0.1) \times 10^{-8}}$	**27.6 / 8**
		PLE	7–228	-29^{+11}_{-10}	$3.8^{+0.3}_{-0.2}$	$2.0 \times 10^{-2\dagger}$	–	35^{+2}_{-4}	$1.7 \times 10^{-8\dagger}$	16.4 / 7
051109A	2005-11-09	XRT	131–196	$0^{\dagger}$	2.2 ± 0.7	3.2×10^{-6}	0.4 / 4	74^{+36}_{-19}	$5.0^{+5.2}_{-2.5} \times 10^{-10}$	0.3 / 10
	01:12:17.6	PL/EX	0–196	1.9	-1.6	2.2×10^{-7}	7.8 / 6	28 ± 1	$(1.5 \pm 0.2) \times 10^{-8}$	50.8 / 8
		PLE	0–196	$\mathbf{4.78 \pm 0.02}$	$\mathbf{0.79 \pm 0.03}$	$\mathbf{2.5 \times 10^{-9\dagger}}$	–	$\mathbf{21 \pm 3}$	$\mathbf{1.5 \times 10^{-8\dagger}}$	**2.8 / 7**
060109	2006-01-09	XRT	110–200	$0^{\dagger}$	4.3 ± 0.4	2.6×10^{-1}	7.3 / 8	33 ± 3	$8.6^{+4.0}_{-2.7} \times 10^{-9}$	8.5 / 8
	16:54:41.2	PL/EX	0–862	88 ± 1	1.6 ± 0.1	$7.1^{+3.7}_{-2.2} \times 10^{-8}$	11.1 / 11	42 ± 2	$(3.6 \pm 0.4) \times 10^{-9}$	109.1 / 12
		PLE	0–862	$\mathbf{90 \pm 0.3}$	$\mathbf{1.42 \pm 0.03}$	$\mathbf{1.8 \times 10^{-8\dagger}}$	–	$\mathbf{32 \pm 2}$	$\mathbf{3.5 \times 10^{-9\dagger}}$	**8.4 / 11**
060111B	2006-01-11	XRT	89–149	$0^{\dagger}$	2.8 ± 0.7	2.1×10^{-5}	2.6 / 3	43^{+14}_{-9}	$6.5^{+6.2}_{-3.3} \times 10^{-10}$	3.2 / 3
	20:15:41.2	PL/EX	0–149	50	2.4	9.3×10^{-7}	13.0 / 6	23 ± 1	$(5.7 \pm 0.7) \times 10^{-9}$	133.3 / 7
		PLE	0–149	$\mathbf{50.1 \pm 0.3}$	$\mathbf{2.38 \pm 0.03}$	$\mathbf{7.5 \times 10^{-7\dagger}}$	–	$\mathbf{13 \pm 2}$	$\mathbf{7.2 \times 10^{-9\dagger}}$	**14.5 / 6**
060202	2006-02-02	XRT	250–350	$0^{\dagger}$	2.2 ± 0.3	8.7×10^{-5}	14.8 / 18	138^{+20}_{-16}	$3.5^{+1.1}_{-0.8} \times 10^{-9}$	15.2 / 18
	08:40:29.9	PL/EX	0–350[a]	135^{+6}_{-8}	1.2 ± 0.2	1.8×10^{-7}	20.0 / 24	141 ± 6	$(3.4 \pm 0.3) \times 10^{-9}$	118.2 / 27
		PLE	0–350	$\mathbf{127 \pm 5}$	$\mathbf{2.4 \pm 0.1}$	$\mathbf{1.3 \times 10^{-5\dagger}}$	–	$\mathbf{141 \pm 5}$	$\mathbf{2.8 \times 10^{-9\dagger}}$	**22.1 / 26**
060211A	2006-02-11	XRT	232–312	$0^{\dagger}$	2.1 ± 0.9	1.6×10^{-5}	5.0 / 6	127^{+96}_{-39}	$8.3^{+12.2}_{-5.0} \times 10^{-10}$	5.2 / 6
	09:39:59.9	PL/EX	0–913	72	2.3	1.7×10^{-5}	43.8 / 29	81 ± 2	$(3.6 \pm 0.2) \times 10^{-9}$	333.0 / 32
		PLE	0–913	**72**	$\mathbf{2.29 \pm 0.02}$	$\mathbf{1.4 \times 10^{-5\dagger}}$	–	$\mathbf{54 \pm 4}$	$\mathbf{3.1 \times 10^{-9\dagger}}$	**39.9 / 31**
060306	2006-03-06	XRT	97–147	$0^{\dagger}$	3.7 ± 0.8	2.2×10^{-3}	3.1 / 2	31^{+9}_{-6}	$1.7^{+2.2}_{-1.0} \times 10^{-9}$	3.3 / 2
	00:49:09.3	PL/EX	35–256	40	2.3	1.1×10^{-6}	31.4 / 4	17.8 ± 0.7	$(3.1 \pm 0.7) \times 10^{-8}$	145.6 / 6
		PLE	35–256	**40**	$\mathbf{2.33 \pm 0.02}$	$\mathbf{1.0 \times 10^{-6\dagger}}$	–	$\mathbf{13 \pm 1}$	$\mathbf{2.5 \times 10^{-8\dagger}}$	**25.4 / 5**
060418	2006-04-18	XRT	178–400	$0^{\dagger}$	2.6 ± 0.1	$3.1^{+3.8}_{-1.7} \times 10^{-4}$	27.1 / 28	101 ± 6	$(2.0 \pm 0.3) \times 10^{-9}$	31.6 / 28
	03:05:49.2[b]	PL/EX	108–797[c]	146 ± 2	1.07 ± 0.08	$2.2^{+1.2}_{-0.8} \times 10^{-8}$	25.0 / 30	262 ± 23	$(3.0 \pm 0.5) \times 10^{-10}$	123.0 / 31
		PLE	108–797[b]	$\mathbf{148.7 \pm 0.3}$	$\mathbf{0.89 \pm 0.01}$	$\mathbf{7.5 \times 10^{-9\dagger}}$	–	$\mathbf{43 \pm 3}$	$\mathbf{1.5 \times 10^{-8\dagger}}$	**23.4 / 30**
060427	2006-04-27	XRT	148–198	$0^{\dagger}$	4.4 ± 1.3	4.8×10^{-1}	3.7 / 3	41^{+20}_{-10}	$5.1^{+14.8}_{-0.3} \times 10^{-9}$	4.0 / 3
	11:43:01.0	PL/EX	0–218	66	2.8	3.7×10^{-5}	3.5 / 3	$\mathbf{47 \pm 2}$	$\mathbf{(2.9 \pm 0.4) \times 10^{-9}}$	**5.1 / 6**
		PLE	0–218	114	6.9	$2.7^{\dagger}$	–	47	$2.8 \times 10^{-9\dagger}$	3.3 / 5
060428B	2006-04-28	XRT	235–340	$0^{\dagger}$	5.0 ± 0.7	74	7.9 / 7	55^{+10}_{-7}	$4.1^{+4.6}_{-2.1} \times 10^{-9}$	9.4 / 7

Table 1—Continued

GRB	t_0 UT	Data‡	Fitting [s]	Power-law					Exponential	
				t_0^{pow}	α	$K_{\rm pow}$	χ^2/dof	w	$K_{\rm exp}$	χ^2/dof
	08:54:15.2	PL/EX	0–340	229	0.7	3.5×10^{-10}	2.9 / 6	**48 ± 0.9**	**8.9×10^{-9}**	**10.4 / 8**
		PLE	0–340	236^{+1}_{-2}	0.40 ± 0.05	6.8×10^{-11}†	2.7 / 7	39 ± 2	1.0×10^{-8}†	2.7 / 7
060923C	2006-09-23	XRT	205–529	0†	2.7 ± 0.3	1.7×10^{-4}	3.5 / 5	115^{+17}_{-14}	4.0×10^{-10}	5.4 / 5
	13:33:10.8	PL/EX	0–529	**-3 ± 2**	**2.76 ± 0.02**	**2.0×10^{-4}†**	**3.5 / 6**	43 ± 1	$(1.3 \pm 0.2) \times 10^{-8}$	45.3 / 6
		PLE	0–529	-2.9 ± 6	2.42 ± 0.03	2.6×10^{-5}†	3.2 / 5	33^{+4}_{-10}	9.5×10^{-9}†	3.2 / 5

‡XRT: only the XRT data fitting with a PLO model and a EXP model, PL/EX: the joint BAT and XRT fitting with a PLO model and a EXP model, PLE: the joint BAT and XRT fitting with a PLEXP model.

†Fixed value.

[a]All the BAT data points and the XRT data from t_0+224 s to t_0+350 s are used in the fitting.

[b]Although *battblocks* found the time interval which is 63 second before t_0, we concluded that this interval is due to the contamination of Sco X-1 in the BAT field of view based on the BAT image analysis.

[c]The fitting data of XRT are from t_0+108 s to t_0+148 s, and from t_0+797 s to t_0+400 s. The BAT data point from t_0+146 s to t_0+156 s are also included in the fits.

Table 2. XRT spectral parameters based on a joint WT and PC data using data above 2 keV. The error in the photon index is in the 90% confidence.

GRB	WT Fitting Range [s]	PC Fitting Range [s]	Γ_{XRT}	χ^2/dof
050803	100.1–184.1	185.5–12976	1.9 ± 0.2	33.0 / 37
050814	166.6–384.9	386.5–14133	2.1 ± 0.2	33.5 / 35
050915B	158.4–313.3	229.9–13791	1.8 ± 0.3	9.3 / 11
051109A	131.4–214.3	3444–17540	2.2 ± 0.2	19.0 / 31
060109	109.8–200.2	201.6–12559	2.0 ± 0.2	23.7 / 21
060111B	89.2–426.7	155.4–12655	2.2 ± 0.3	10.0 / 14
060202	175.1–1025	1028–13027	$1.99^{+0.05}_{-0.04}$	364.6 / 337
060211A	137.1–330.9	332.5–13054	1.8 ± 0.1	68.6 / 66
060306	96.9–174.5	175.8–12874	2.40 ± 0.03	9.8 / 15
060418	166.1–697.7	699.9–12561	$2.00^{+0.07}_{-0.06}$	211.7 / 209
060427	148.2–236.5	237.9–12691.	2.0 ± 0.4	7.7 / 10
060428B	235.6–440.8	442.7–12773	2.6 ± 0.3	16.6 / 17
060923C	204.6–267.4	268.7–12796	2.1 ± 0.4	3.0 / 7

Table 3. BAT prompt emission properties. Errors in the 68% confidence.

GRB	T_{90} [s]	Model⋆	Γ_{BAT}	$E_{\rm peak}$ [keV]	$S_E{}^a$	$F_E^{peak\,b}$	S3/S2[c]	z	$T_{1/2}$	$\gamma^\ddagger$	R_0 [cm]	α_{tail}	χ^2/d.o.f.
050803	87.9	PL	1.39 ± 0.07	–	22 ± 1	8.1 ± 0.7	1.5 ± 0.1	–	18	270	2.8×10^{16}	–	–
050814	140.6	PL	1.8 ± 0.1	–	19 ± 1	6.2 ± 1.2	1.2 ± 0.1	5.3[1]	45	240	3.0×10^{16}	–	–
050915B	40.9	CPL	1.4 ± 0.2	60^{+7}_{-5}	34 ± 1	17 ± 1	1.05 ± 0.04	–	24	242	3.0×10^{16}	–	–
051109A	37.2	PL	1.5 ± 0.1	–	22 ± 2	29 ± 3	1.4 ± 0.2	2.346[2]	15	287	2.7×10^{16}	0.59 ± 0.05	9.7 / 14
060109	115.4	PL	1.9 ± 0.1	–	6.6 ± 0.6	3.4 ± 0.1	1.0 ± 0.2	–	23	246	3.0×10^{16}	–	–
060111B	58.8	PL	1.0 ± 0.1	–	16 ± 1	14 ± 2	2.0 ± 0.1	–	9	350	2.4×10^{16}	0.9 ± 0.1	1.0 / 3
060202	198.9	PL	1.8 ± 0.1	–	22 ± 1	3.7 ± 0.8	1.2 ± 0.1	–	98	143	4.3×10^{16}	–	–
060211A	126.3	CPL	0.9 ± 0.3	58^{+8}_{-5}	16 ± 1	3.3 ± 0.1	1.1 ± 0.1	–	24	242	3.0×10^{16}	1.3 ± 0.2	1.0 / 2
060306	61.2	PL	1.80 ± 0.05	–	21 ± 1	47 ± 2	1.1 ± 0.1	–	46	190	3.5×10^{16}	1.2 ± 0.2	2.4 / 3
060418	103.1	PL	1.64 ± 0.03	–	80 ± 1	49 ± 2	1.28 ± 0.03	1.489[3]	21	226	3.1×10^{16}	–	–
060427	64	PL	1.9 ± 0.2	–	5.0 ± 0.5	1.7 ± 0.7	1.1 ± 0.2	–	32	217	3.2×10^{16}	–	–
060428B	57.9	PL	2.6 ± 0.1	–	8.2 ± 0.5	3.4 ± 0.6	0.7 ± 0.1	–	27	232	3.1×10^{16}	3.0 ± 0.3	4.7 / 8
060923C	75.8	PL	2.3 ± 0.1	–	16 ± 1	5.0 ± 1.5	0.8 ± 0.1	–	–	–	–	–	–

⋆PL: power-law ($dN/dE \sim E^{-\Gamma_{BAT}}$), CPL: cutoff power-law ($dN/dE \sim E^{-\Gamma_{BAT}} \exp(-(2-\Gamma_{BAT})E/E_{\rm peak})$)

‡Calculated bulk Lorentz factor assuming $E_0/n = 1 \times 10^{52}$ erg cm^3.

[a]Energy fluence in the 15–150 keV band [10^{-7} erg cm^{-2}]

[b]1-s peak energy flux in the 15–150 keV band [10^{-8} erg cm^{-2} s^{-1}]

[c]Fluence ratio between S3(50–150 keV)/S2(25–50 keV)

[1]Jakobsson et al. (2006)

[2]Quimby et al. (2005)

[3]Dupree et al. (2006)

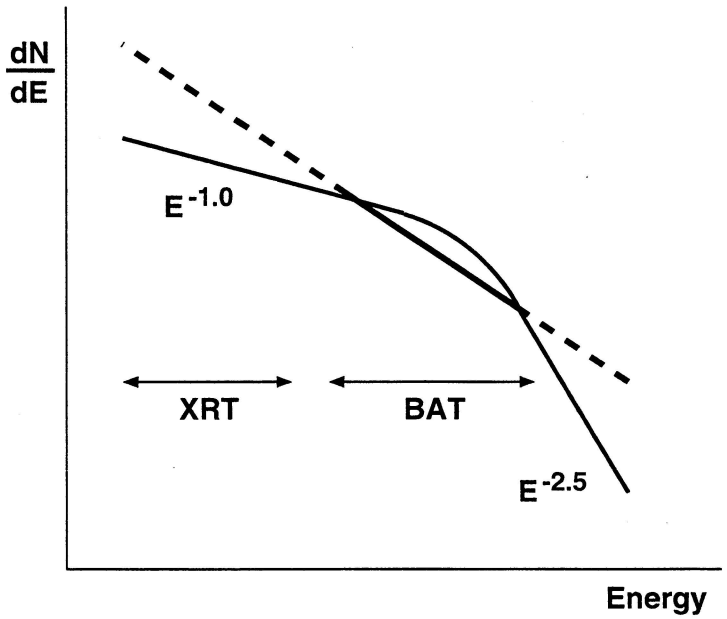

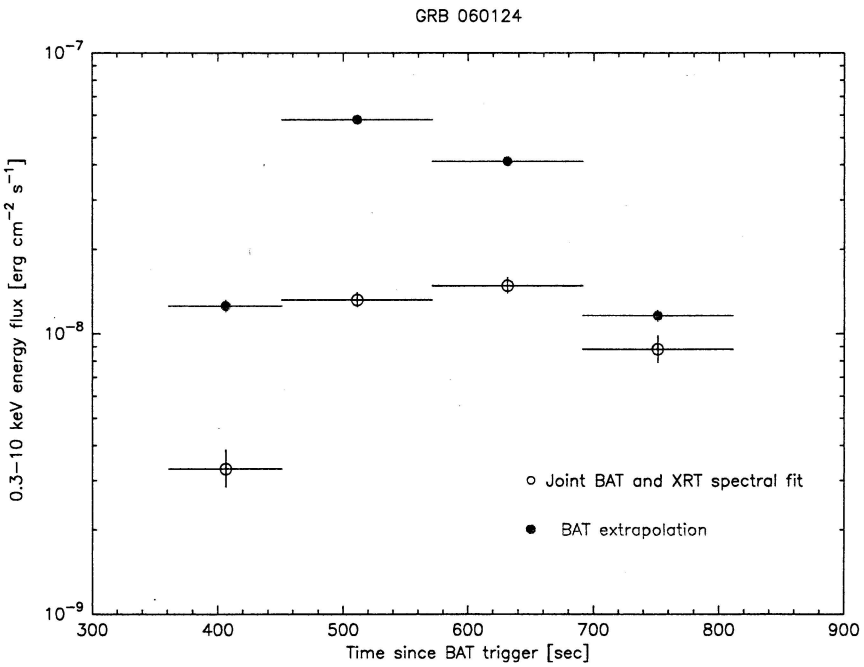

Fig. 1.— Top: Schematic figure of the observed count spectrum. If the curvature of the GRB spectrum is within the BAT energy range, BAT observed photon index in a simple power-law will be steeper than the actual photon index observed in the XRT energy range. Bottom: The light curve of the main emission of GRB 060124. The 0.3–10 keV flux of the black open circles are derived from the joint spectral analysis of BAT and XRT. The red filled circles are derived from extrapolating the BAT mask-weighted count rate in the full energy band to 0.3–10 keV using the averaged photon index of the BAT and XRT PC mode spectrum.

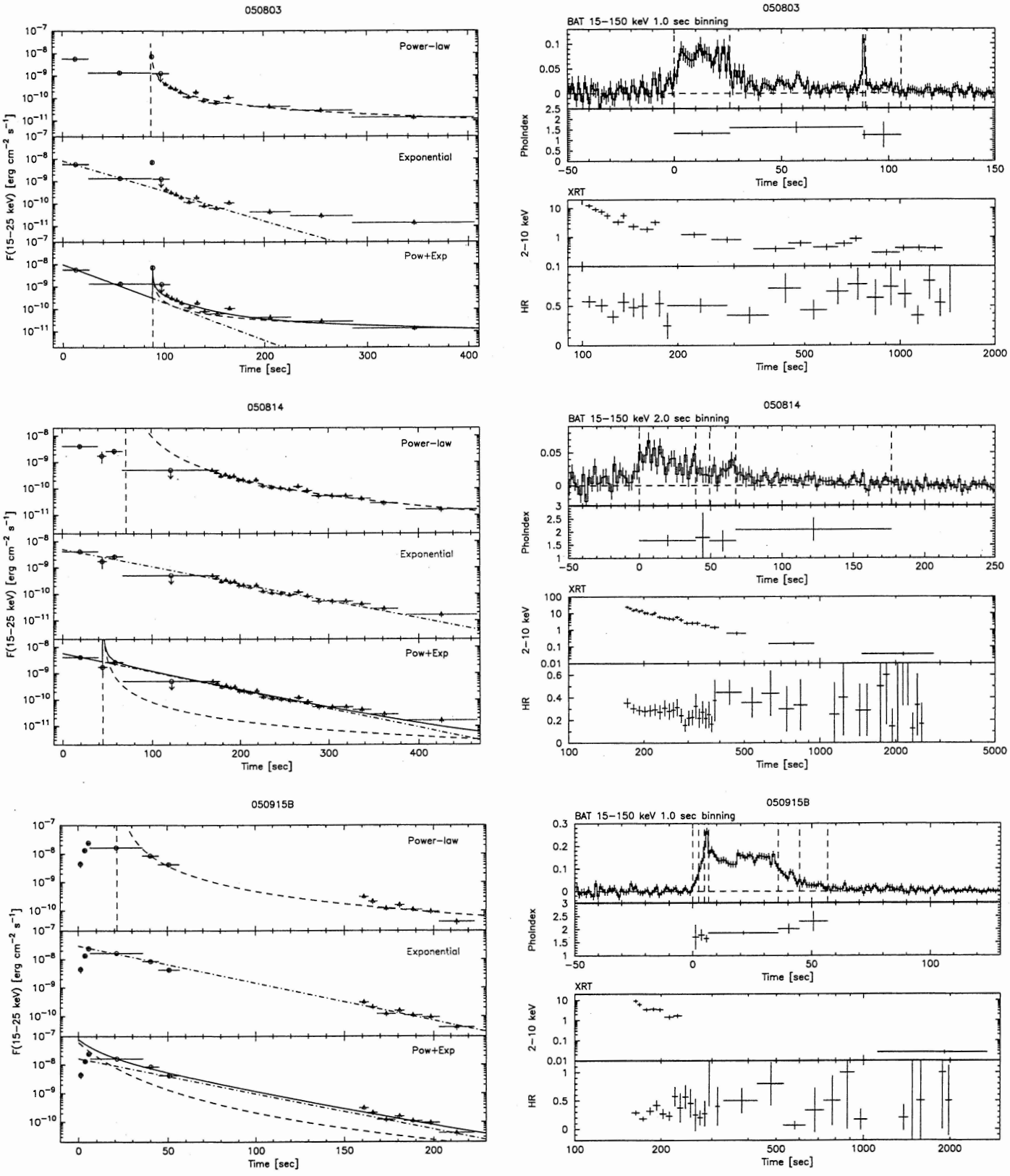

Fig. 2.— The BAT and XRT composite light curve (see details in the text).

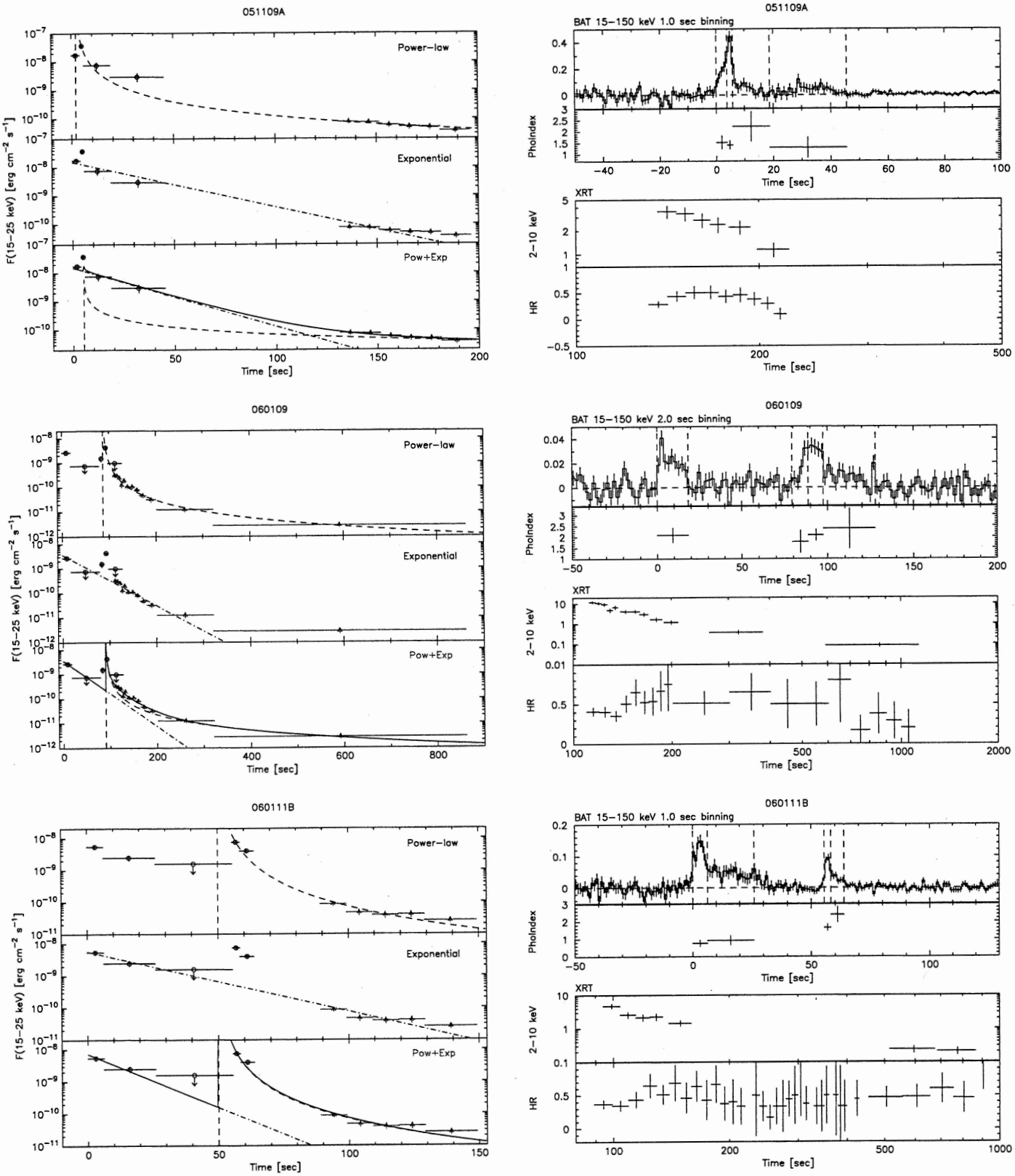

Fig. 2.— continued.

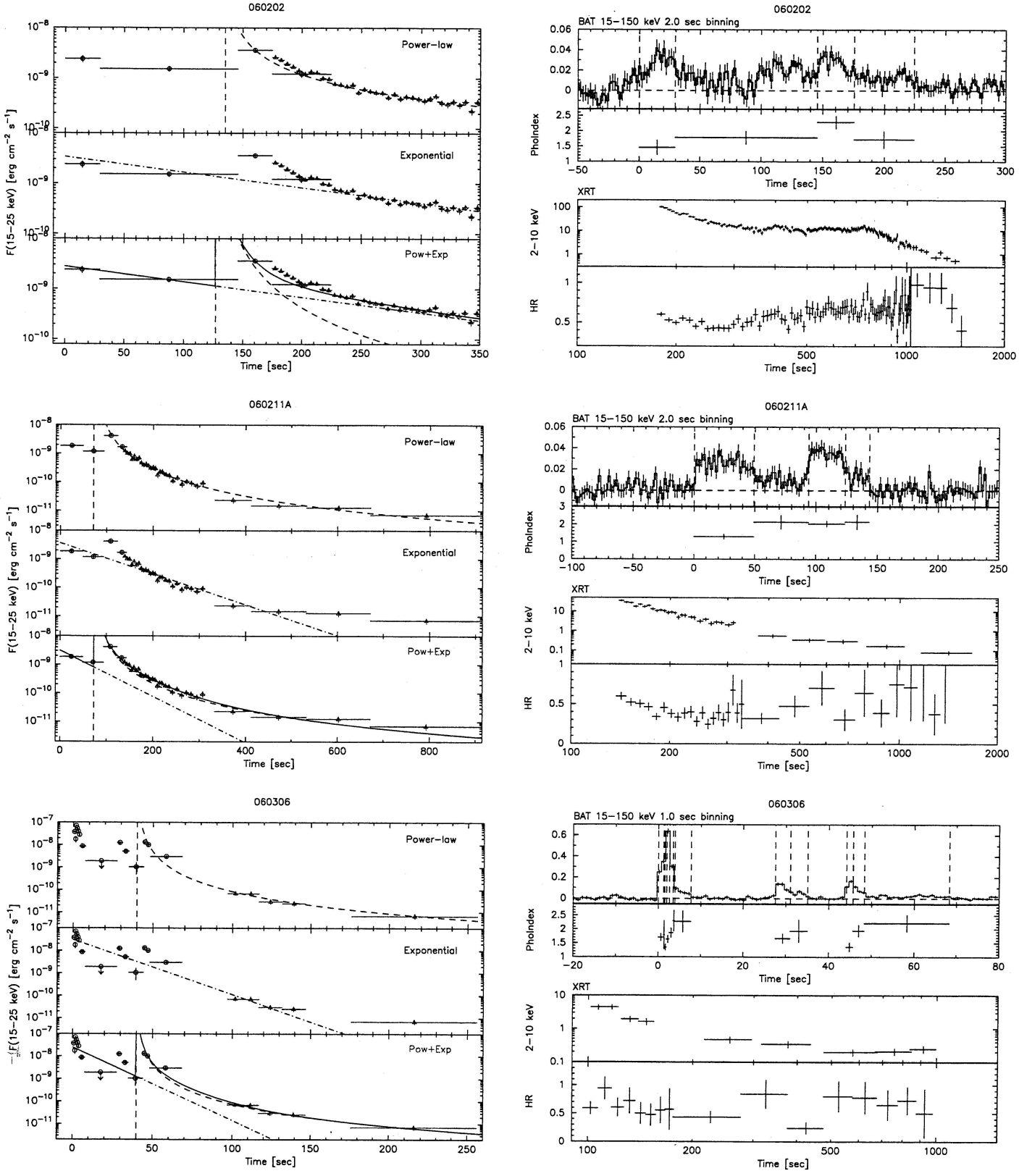

Fig. 2.— continued.

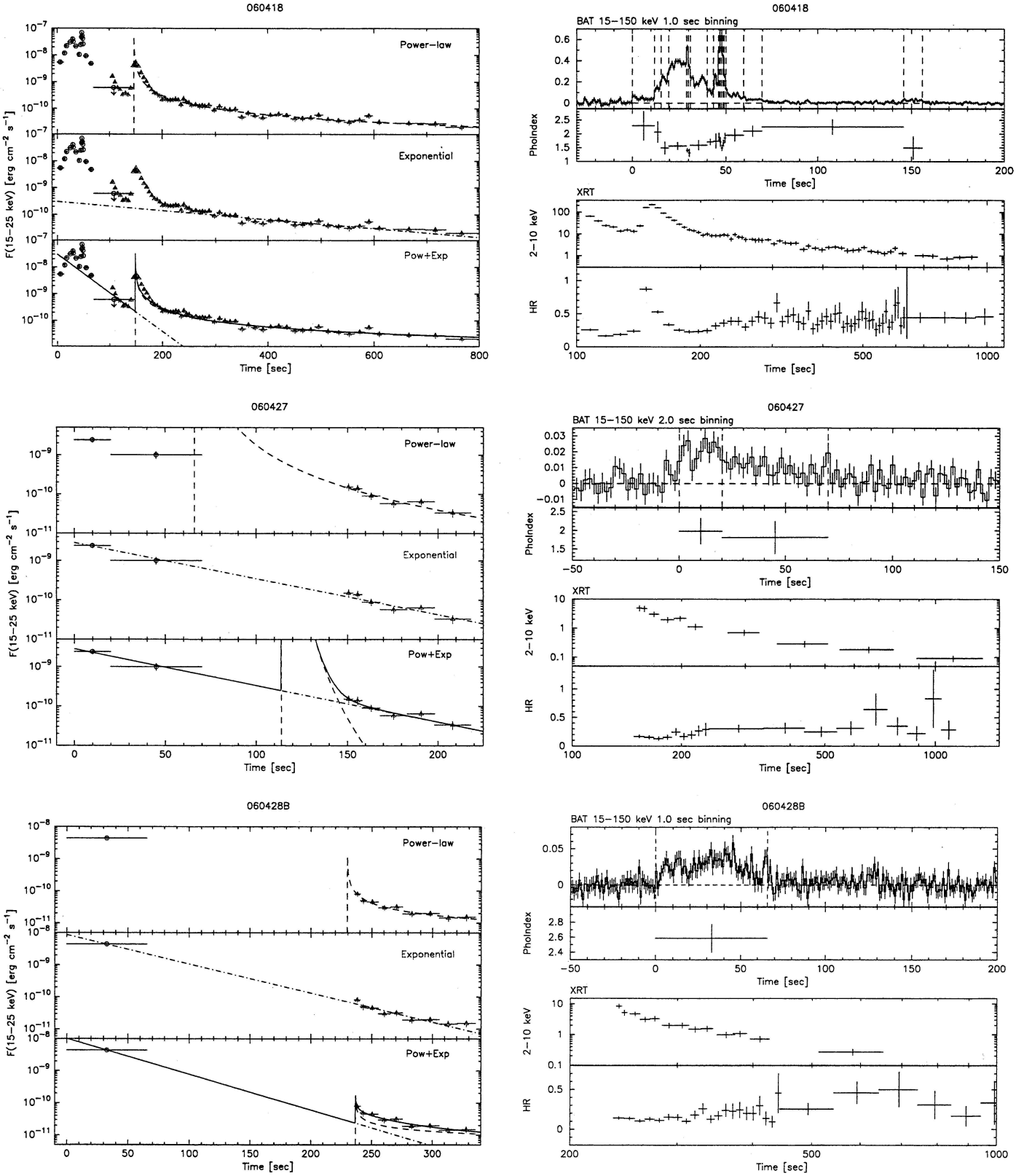

Fig. 2.— continued.

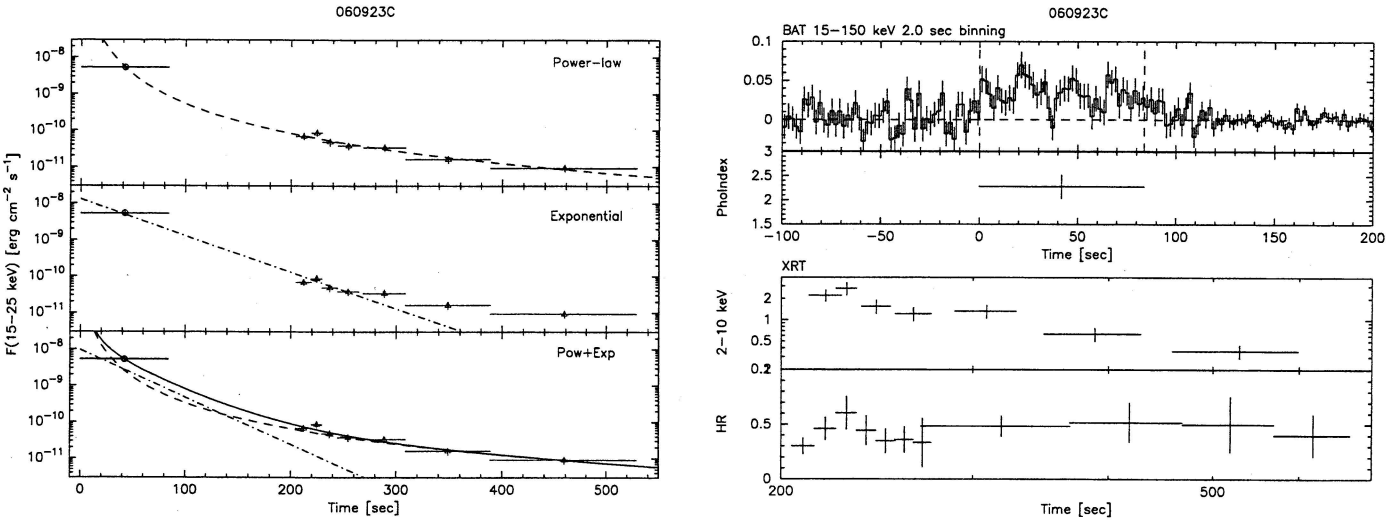

Fig. 2.— continued.

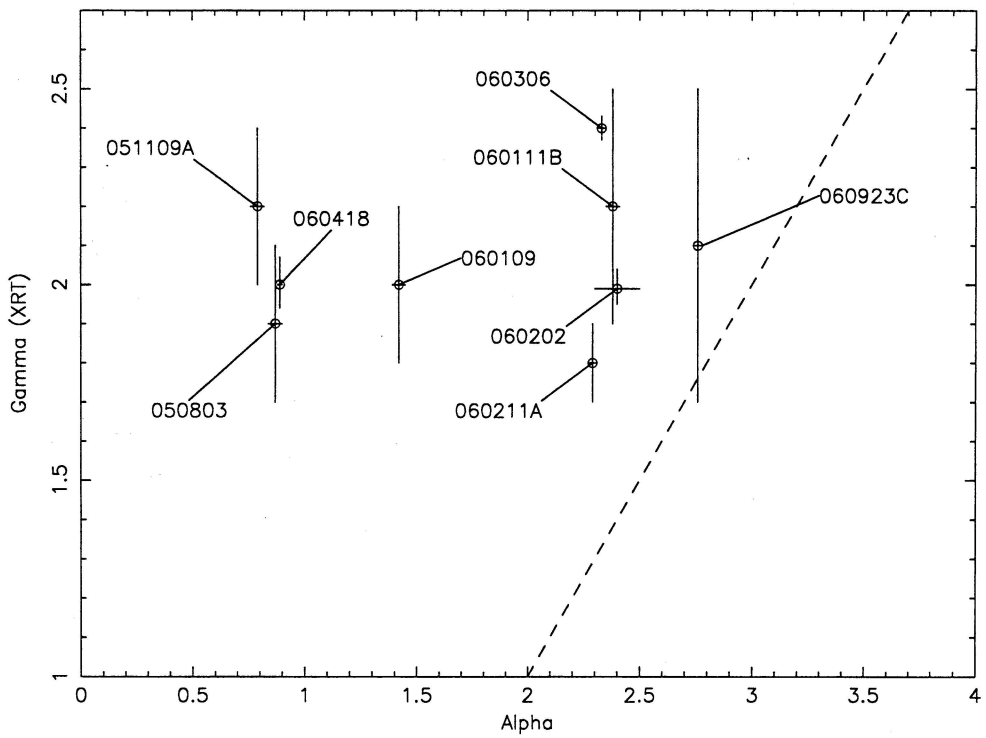

Fig. 3.— The correlation between the power-law decay index, α, of the light curve and a photon index, Γ_{XRT}. The dashed line is the expected relationship from the curvature effect ($\alpha = 1 + \Gamma_{XRT}$).

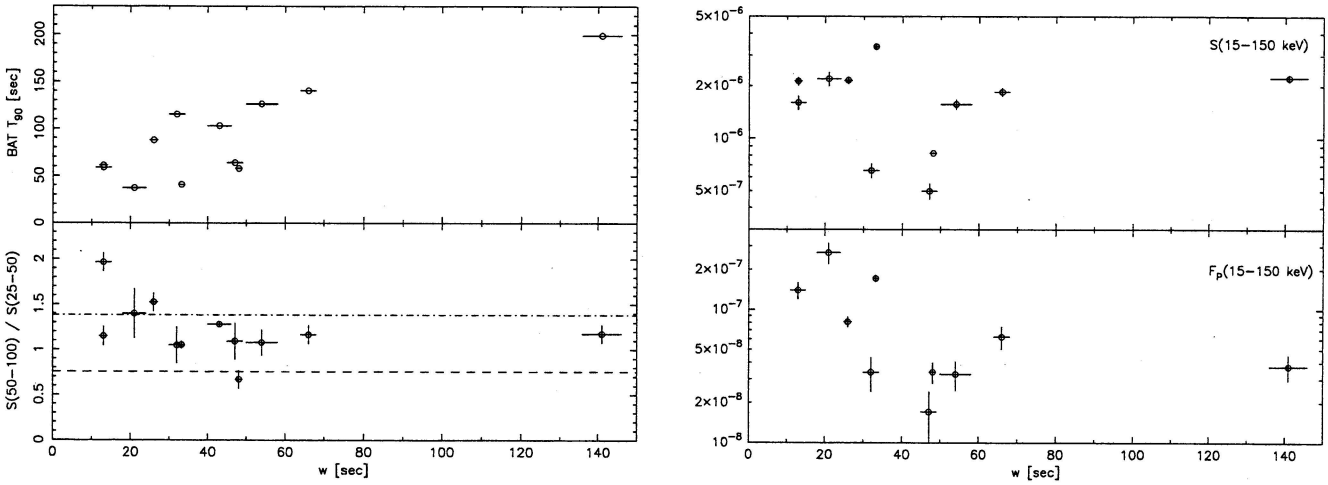

Fig. 4.— The correlation between the decay constant, w, of an exponential model and the BAT prompt emission properties. Left top: w vs. BAT T_{90}, Left bottom: w vs. the fluence ratio between the 50-100 keV and 25-50 keV band (the dotted and dash-dotted lines are the calculation assuming $E_{\rm peak} = 30$ keV and $E_{\rm peak} = 100$ keV, respectively, with $\alpha = -1.0$ and $\beta = -2.5$ in the Band function), Right top: w vs. the fluence in the 15-150 keV band, Right bottom: w vs. the 1-s peak flux in the 15-150 keV band.

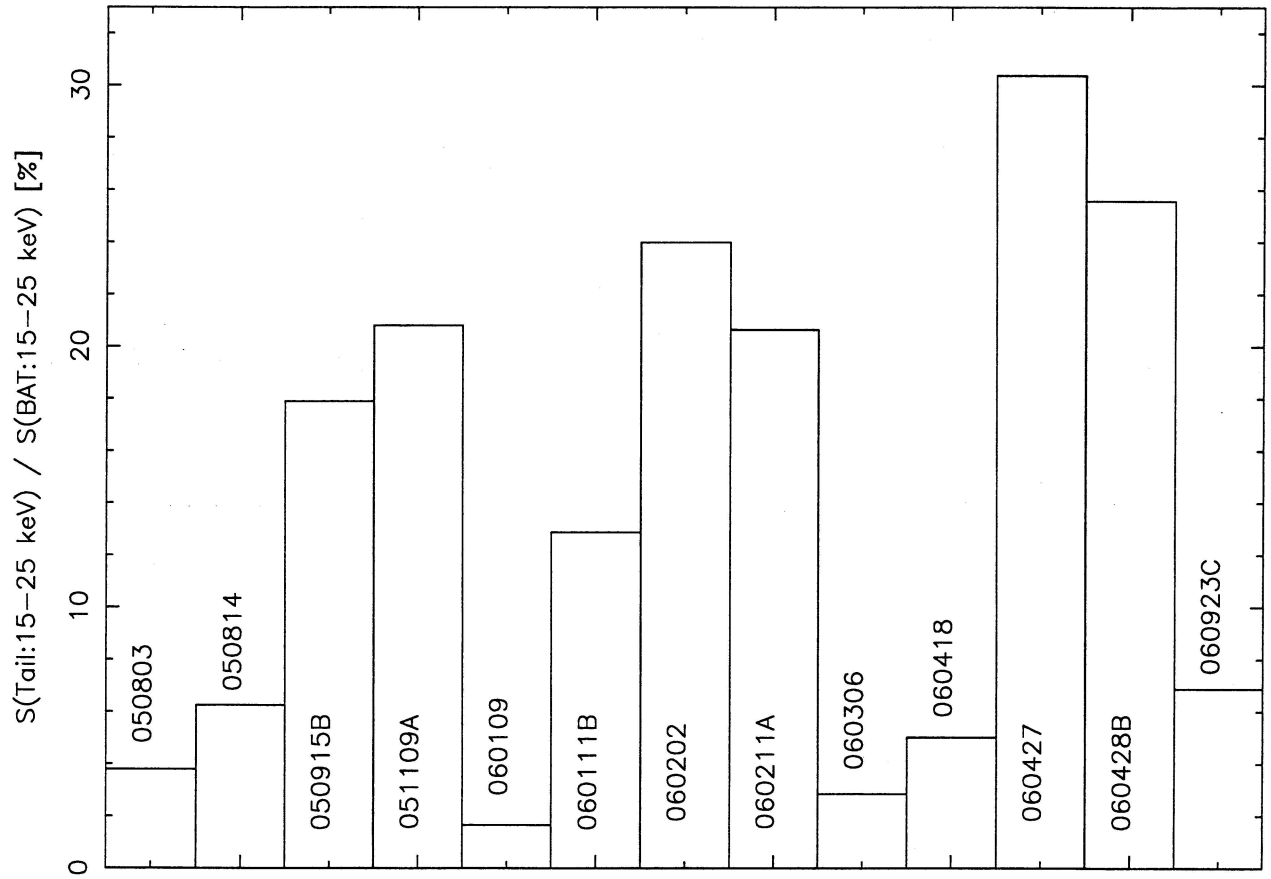

Fig. 5.— The histogram of the ratio in percent between the fluence accumulated from the end of the emission detected by the BAT to 1000 s after t_0 (S(Tail:15-25 keV)) and the fluence recored by the BAT (S(BAT:15-25 keV)).